

Theory of a one-dimensional double-X atom interferometer

Marvin D. Girardeau,* Kunal K. Das,† and Ewan M. Wright‡

Optical Sciences Center and Department of Physics, University of Arizona, Tucson, AZ 85721

(Dated: March 10, 2021)

The dynamics of an atom waveguide X-junction beam splitter becomes truly 1D in a regime of low temperatures and densities and large positive scattering lengths where the transverse mode becomes frozen and the many-body Schrödinger dynamics becomes exactly soluble via a generalized Fermi-Bose mapping theorem. We analyze the interferometric response of a double-X interferometer of this type due to potential differences between the interferometer arms.

PACS numbers: 03.75.Fi,03.75.-b,05.30.Jp

I. INTRODUCTION

Recent advances in atom de Broglie waveguide technology [1, 2, 3, 4, 5] and its potential applicability to atom interferometry [6] and integrated atom optics [3, 7] create a need for accurate theoretical modelling of such systems in the low temperature, tight waveguide regime where transverse excitations are frozen out and the quantum dynamics becomes essentially one-dimensional (1D) (Tonks-gas limit). It has been shown by Olshanii [8], and also by Petrov et al. [9], that at sufficiently low temperatures and densities and high transverse frequencies ω_0 , where thermal and longitudinal zero-point energies are small compared with $\hbar\omega_0$, the transverse degrees of freedom of a Bose-Einstein condensate (BEC) in an atom waveguide are frozen in the ground transverse mode and the dynamics becomes one-dimensional. If, in addition, the scattering length is large and positive, the dynamics reduce to those of a 1D gas of hard core, or impenetrable, point bosons [8, 9]. This is a model for which the exact many-body energy eigensolutions were found in 1960 using an exact mapping from the Hilbert space of energy eigenstates of an ideal gas of spinless fermions to that of many-body eigenstates of hard core, and therefore strongly interacting, bosons [10, 11]. Recently two of us have extended this mapping technique in order to treat the exact many-body dynamics of Tonks gases [12, 13] and the exact many-body ground-state of a trapped Tonks gas [14].

“Waveguide on a chip” technology [15, 16] has already advanced to achievement of BEC on a magnetic surface microtrap [17] and construction of a Y-beam splitter on a chip [18], and the theory of a multimode double-Y interferometer has been developed [19] in an approximation where atomic interactions are neglected. Here we are interested in the the opposite limit of the Tonks-gas regime [8, 9] where interatomic interactions and two-body correlations play a major role. Such a study is motivated by our previous demonstration [13] that fermionization

strongly inhibits interference in an adiabatically split and recombined Tonks gas. The Fermi-Bose mapping and dynamics of a pulsed interferometer are more complicated and it is not clear a priori whether significant interference effects will occur in this case. This motivates the present investigation.

We set up our model for the double-X interferometer in Section II as an effective 1D problem. In Sec. III A we develop a generalized mapping theorem and thereby map the Tonks state to a 1D Fermi gas of free fermions, in Sec. III B we define the boundary conditions at the junctions in terms of single particle wave functions, and in the remainder of Sec. III we examine the limits of validity of the model and we develop a general expression for the bosonic spatial density profiles in terms of simpler Fermi orbitals which are not subject to the X-splitter boundary conditions. Analytical expressions for the interferometric response are developed in Sec. IV and numerical results are presented in Sec. V.

II. DOUBLE-X INTERFEROMETER

The interferometer model of Andersson *et al.* [19] consists of an atom waveguide which is first split into two identical waveguides by a symmetrical Y-junction, followed by a reverse Y-junction which recombines the output of the two arms into a single waveguide, the “exit port”, where interference fringes appear as a result of potential differences between the two interferometer arms. The emphasis there was on effects of multi-transverse-mode propagation, assuming the transverse trap frequency low enough and/or longitudinal density high enough and/or temperature high enough that many transverse modes of the guides are energetically accessible and many-body correlations are negligible. In the opposite Tonks limit where the transverse wave function is frozen, the dynamics fermionizes and multiple longitudinal modes play a crucial role, due to the Fermi-Bose mapping theorem [10, 11, 12, 13, 14] which introduces a Fermi sea of many longitudinal orbitals into the many-boson dynamics. Rather than the double-Y geometry of Andersson *et al.*, we assume a double-X geometry since its greater symmetry and reversibility makes implementation of unitary straightforward; It is essentially the same

*Electronic address: girardeau@optics.arizona.edu

†Electronic address: kdas@optics.arizona.edu

‡Electronic address: Ewan.Wright@optics.arizona.edu

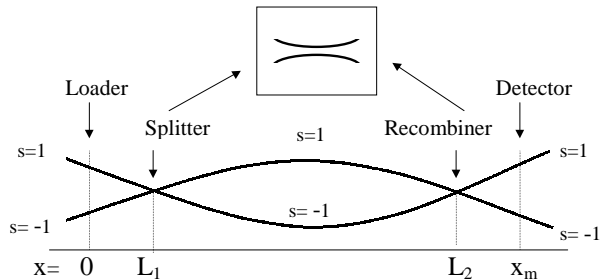


FIG. 1: Schematic diagram of the interferometer. The inset shows that the junctions are actually avoided crossings with tunnelling between the waveguides.

model used by Scully and Dowling [20, 21] in their treatment of an atom waveguide analog of a Mach-Zehnder optical interferometer. We assume that the entrance arms, upper and lower arms after the X-splitter, and exit arms after the X-recombiner all satisfy the necessary and sufficient conditions for the Tonks regime [8, 9]. We can retain an effective 1D description despite the splitting and recombination (a) by assuming that corresponding upper and lower interferometer arms have the same length, so that the same longitudinal coordinate x can be used for both arms and (b) by introducing a pseudospin representation with $s = 1$ (-1) labelling atoms in the upper (lower) interferometer arm. Our basic model of a double-X interferometer is shown in Fig. 1, and we remark that the same model applies to an atomic loop mirror employing an X-input-coupler. The inset indicates that the two apparent X-crossings are really “avoided crossings” of the waveguides, with tunneling between the two in their regions of near tangency. We idealize these tunneling regions to points, see discussion following Eq. (9), taking the X-splitter to be at $x = L_1$ and X-recombiner at $x = L_2$ and treating the effects of tunneling by boundary conditions specifying the wave function discontinuities at these two points. Then x specifies the position of an atom in one of the entrance arms if $x < L_1$, one of the interferometer arms if $L_1 < x < L_2$, and one of the exit arms if $x > L_2$. Details of these boundary conditions will be given in the following section.

III. THEORETICAL MODEL

A. Generalized Mapping Theorem

Our objective is to find dynamical solutions for an N -boson Tonks gas in the X-splitter geometry which are exact solutions of the time-dependent many-body Schrödinger equation (TDMBSE) except when any of the N particle positions x_j is equal to L_1 or L_2 (X-junctions),

satisfy a point hard core impenetrability constraint, have Bose symmetry (totally symmetric), and include the effect of tunneling at the X-junctions via appropriate boundary conditions. We do this by generalizing our previous Fermi-Bose mapping theorem [10, 11, 12, 13, 14] to the present more complicated geometry.

A system of N atoms is described by solutions $\Psi(x_1, s_1; \dots; x_N, s_N; t)$ of the TDMBSE $\hat{H}\Psi = i\hbar\partial\Psi/\partial t$. In the Tonks limit (large scattering length, low linear density, tight transverse confinement) [8, 9] the two-particle interaction behaves as a hard core of vanishing diameter $a \rightarrow 0$. This is conveniently treated as a constraint on allowed wave functions:

$$\Psi = 0 \text{ if } s_j = s_k \text{ and } x_j = x_k, \quad 1 \leq j < k \leq N, \quad (1)$$

implying that atoms in the same arm cannot interpenetrate whereas those in different arms have no such constraint. We start from fermionic solutions $\Psi_F(x_1, s_1; \dots; x_N, s_N; t)$ of the TDMBSE which are antisymmetric under all space-pseudospin pair exchanges $(x_j, s_j) \leftrightarrow (x_k, s_k)$, hence all permutations. Generalizing the previous definition [10, 11, 12, 13, 14], define a “unit antisymmetric function” A by

$$\begin{aligned} A(x_1, s_1; \dots; x_N, s_N) &= \prod_{1 \leq j < k \leq N} \alpha(x_j, s_j; x_k, s_k) \\ \alpha(x_j, s_j; x_k, s_k) &= \delta_{s_k, s_j} \text{sgn}(x_k - x_j) \\ &\quad + \delta_{s_j, 1} \delta_{s_k, -1} - \delta_{s_j, -1} \delta_{s_k, 1}, \end{aligned} \quad (2)$$

where $\text{sgn}(x) = +1(-1)$ if $x > 0(x < 0)$. For a given antisymmetric Ψ_F , define a bosonic wave function Ψ_B by

$$\begin{aligned} \Psi_B(x_1, s_1; \dots; x_N, s_N; t) &= A(x_1, s_1; \dots; x_N, s_N) \\ &\quad \times \Psi_F(x_1, s_1; \dots; x_N, s_N; t). \end{aligned} \quad (3)$$

It satisfies the impenetrability constraint (1) because any spinless fermion wave function is space-antisymmetric under exchange of like-pseudospin pairs. It is totally symmetric (bosonic) under space-pseudospin permutations, obeys the same boundary conditions as Ψ_F , and the Bose TDMBSE $\hat{H}\Psi_B = i\hbar\partial\Psi_B/\partial t$ follows from the Fermi one $\hat{H}\Psi_F = i\hbar\partial\Psi_F/\partial t$ by straightforward generalization of the previous argument [10, 11, 12, 13, 14], under the assumption that the Hamiltonian is the sum of kinetic energy operators and ordinary (non-operator) potentials. These potentials may depend on pseudospin, i.e., they may differ between the left and right interferometer arms, as is the case in modelling interferometric detectors. Since the only interatomic interaction in the Tonks limit is the point hard core created by the constraint (1), and this constraint is satisfied automatically by the N -fermion wave functions Ψ_F in (3) as a consequence of their antisymmetry, it follows that Ψ_F is a dynamical ideal Fermi gas state which can be written as a Slater determinant

$$\Psi_F(x_1, s_1; \dots; x_N, s_N; t) = \frac{1}{\sqrt{N!}} \det_{n,j=1}^N \phi_n(x_j, s_j; t), \quad (4)$$

where ϕ_n are N orthonormal solutions of the *single-particle* TDSE.

B. X-splitter boundary conditions

The TDMBSE is

$$\left[\sum_{j=1}^N \left(-\frac{\hbar^2}{2m} \frac{\partial^2}{\partial x_j^2} + V_s(x_j, t) \right) - i\hbar \frac{\partial}{\partial t} \right] \Psi = 0, \quad (5)$$

where $V_s(x, t)$ are longitudinal potentials assumed to be nonzero only within the interferometer arms $L_1 < x < L_2$. The mapping theorem guarantees that Ψ_B will satisfy this TDMBSE at all points $(x_1, s_1; \dots; x_N, s_N)$ where Ψ_F does. However, Ψ_F and hence Ψ_B fail to satisfy the TDMBSE at the points $x_j = L_1$ and $x_j = L_2$ where tunneling introduces discontinuities in the wave function; at these points the TDMBSE is replaced by boundary conditions specifying the discontinuities. Each of the orbitals in the fermionic solution (4) of the TDMBSE (5) satisfies the *single-particle* TDSE

$$\left[-\frac{\hbar^2}{2m} \frac{\partial^2}{\partial x^2} + V_s(x, t) - i\hbar \frac{\partial}{\partial t} \right] \phi_n(x, s; t) = 0, \quad (6)$$

everywhere except at the X-junctions $x = L_1$ and $x = L_2$, where this TDSE is replaced by a boundary condition. Since evolution according to the TDSE is unitary, the transformation from the left to the right side of each junction can be implemented by a unitary 2×2 matrix. Assume that at the junction half of the probability initially in the upper arm remains in the upper ($s = 1$) arm and half tunnels to the lower arm, and similarly for probability entering from the lower arm, and introduce a Pauli pseudospinor notation

$$\Phi_n(x, t) = \begin{bmatrix} \phi_n(x, +1; t) \\ \phi_n(x, -1; t) \end{bmatrix}. \quad (7)$$

Then a simple boundary condition which implements the splitting at the first X-junction is [20, 22]

$$\Phi_n(L_1+, t) = \mathbf{T} \Phi_n(L_1-, t), \quad (8)$$

where $L_1- (L_1+)$ denotes the left (right) side of the junction and \mathbf{T} is the unitary matrix

$$\mathbf{T} = \frac{1}{\sqrt{2}} \begin{pmatrix} 1 & -1 \\ 1 & 1 \end{pmatrix}. \quad (9)$$

Thus the amplitudes which remain in the upper or lower arms as they pass through the avoided crossing junction suffer no phase shifts, that which tunnels from the upper to the lower arm suffers a phase shift of π , and that which tunnels from the lower to the upper arm suffers no phase change. It can be shown that this matrix can be written in the form $e^{i\hat{V}} = (1/\sqrt{2})(1 - \hat{\sigma}_+ + \hat{\sigma}_-)$ in terms of an interaction $\hat{V} = i\lambda(\hat{\sigma}_+ - \hat{\sigma}_-)$ where $\hat{\sigma}_{\pm}$ are Pauli

pseudospin raising and lowering operators implementing the tunneling and λ is taken equal to $\pi/4$ in order that probability splits equally between the upper and lower arms. More general phase shifts could be used subject to the proviso that \mathbf{T} must be unitary, but the simple choice here is sufficient. At the recombiner ($x = L_2$) the same matrix boundary condition is applied once more to generate the amplitudes in the upper and lower output arms.

C. Limits of validity

In our simple model the tunneling regions giving rise to the X-splitters are replaced by point boundary conditions, and we now examine the conditions for this to be valid. In particular, in the boundary condition (8) we treat each orbital separately, meaning that the tunneling is assumed to proceed as for single particles and to not be modified by many-body interactions. For a 50:50 X-splitter, and assuming a tunneling region length L_{coup} , the energy splitting $\Delta E \ll \hbar\omega_0$ between the symmetric and anti-symmetric transverse modes of the tunnel-coupled waveguides must obey $(\Delta E/\hbar) \cdot (L_{coup}/v_x) = \pi/4$, where v_x is the longitudinal velocity of the atoms entering the X-splitter. Here L_{coup}/v_x is the time of flight of the atoms through the tunneling regions, and the $\pi/4$ phase-difference between the modes is that required for a 50:50 splitter. For single-particle tunneling to be valid we require that the energy splitting is large compared to the many-body energy per particle of the incoming Tonks gas of mean density ρ , $\Delta E \gg \hbar^2\pi^2\rho^2/6m$ [10, 11]. When this condition is satisfied the atoms tunnel individually and the transfer characteristics of the X-splitter should therefore be the same for bosons and fermions. For an initial gas in its ground-state which is harmonically trapped with longitudinal frequency ω we have $\rho \approx N/x_F$, where $x_F = \sqrt{2N}x_{osc}$, $x_{osc} = \sqrt{\hbar/m\omega}$ being the single particle ground-state width [23]. In order that the tunneling region not create large density gradients in the atomic gas we also require $L_{coup} \geq x_F$, that is the coupling region is longer than the width of the initial trapped gas. Furthermore, under the assumption $L_{coup} \ll (L_2 - L_1)$ we may treat the tunnel regions as points. Combining these results together, we obtain the following conditions for the action of the X-splitters to be treated by the boundary condition (8)

$$v_x \gg N \cdot L_{coup} \cdot \omega \quad (10)$$

$$(L_2 - L_1) \gg L_{coup} \geq \sqrt{2N}x_{osc}. \quad (11)$$

We shall hereafter assume these conditions are satisfied.

D. Construction of interferometer solutions

The boundary conditions (8) at the X-splitters can be implemented as follows: Let $u_n(x, s; t)$ be solutions on

$x \in [-\infty, \infty]$ of the same single-particle TDSE (6) as the $\phi_n(x, s; t)$ satisfy, but now *no boundary condition* is imposed on these orbitals, so they are continuous with continuous gradient at all x including $x = L_1$ and $x = L_2$. Instead, an initial condition

$$u_n(x, s; t = 0) = u_n(x), \quad (12)$$

is imposed. Note that this initial condition is independent of s (the same in both entrance arms). Here $t = 0$ is a time shortly after loading of the N atoms into the entrance arm and the $u_n(x)$, defined for $1 \leq n \leq N$, are a set of orthonormal orbitals which are negligible at $t = 0$ for $x \geq L_1$. Then for $t \geq 0$ and $x < L_1$, define new orbitals ϕ_n by

$$\phi_n(x, s; t) = u_n(x, s; t)\delta_{s1}, \quad x < L_1. \quad (13)$$

These ϕ_n , which in our model represent the actual orbitals occupied by the atoms, satisfy the same TDSE (6) as the u_n for $x < L_1$, but they are nonvanishing only in the upper arm ($s = 1$), corresponding to our assumption that the atoms are to be loaded only into the upper arm. On the other hand, the u_n are nonzero in both the upper and lower arms as a consequence of their initial conditions (12) and TDSE (6). This allows us to first solve the TDSE without imposing boundary conditions at the junctions $x = L_1$ and $x = L_2$, then construct solutions ϕ_n of the TDSE satisfying the proper boundary conditions by defining them in terms of the u_n by definitions which are properly discontinuous at the junctions. The effect of the boundary condition at $x = L_1$ is such that the upper-arm amplitude $u_n(L_1, 1; t)$ splits equally, with prefactors $1/\sqrt{2}$, between the upper and lower arms at the junction. Note that $u_n(L_1, 1; t) = u_n(L_1, -1; t)$ since V_s vanishes for $x < L_1$ and the initial condition (12) is independent of s . It then follows that the solutions of the TDSE in the interferometer arms are simply

$$\Phi_n(x, t) = \frac{1}{\sqrt{2}} \begin{bmatrix} u_n(x, 1; t) \\ u_n(x, -1; t) \end{bmatrix}, \quad L_1 < x < L_2 \quad (14)$$

In general these u_n depend on $s = \pm 1$ since the potentials V_s in the arms $L_1 < x < L_2$ do.

At the recombiner $x = L_2$ the splitting matrix \mathbf{T} is applied once more, resulting in the solutions

$$\Phi_n(x, t) = \frac{1}{2} \begin{bmatrix} u_n(x, 1; t) - u_n(x, -1; t) \\ u_n(x, 1; t) + u_n(x, -1; t) \end{bmatrix}, \quad x > L_2 \quad (15)$$

in the output arms, where the potentials V_s are again zero.

The above equations uniquely and straightforwardly determine the many-fermion wave function Ψ_F in terms of N orbitals ϕ_n . Then within the limits of validity of our theory given in Sec. (III C), under which the tunneling occurs as for single-particles and is hence the same for bosons and fermions, the many-boson wave function is given by $\Psi_B = A\Psi_F$. Since $A^2 = 1$, this has the important consequence that the single-particle densities

$\rho(x, s; t)$ are the same for the Bose Tonks gas as for the ideal “spinless” Fermi gas of the mapping theorem, allowing us to compute Bose dynamics and interference fringes for this model of a Tonks gas interferometer in terms of the corresponding solutions for the ideal Fermi gas. This will be done in the following sections. In addition to providing the basis for an exact calculation of the behavior of a Tonks gas of bosonic atoms in this interferometer model via the Fermi-Bose mapping theorem, this fermionic calculation is of interest in its own right, since a spin-polarized Tonks gas of fermionic atoms is dynamically equivalent to the same ideal Fermi gas inasmuch as it satisfies the impenetrability constraint (1) automatically as a consequence of spatial antisymmetry.

E. Construction of spatial density profiles

It follows from orthonormality of the $u_n(x)$ and the unitarity of Schrödinger evolution that the $u_n(x, s; t)$ satisfy the orthonormality relation $\int_{-\infty}^{\infty} u_n^*(x, s; t)u_m(x, s; t)dx = \delta_{nm}$ for each fixed $s = \pm 1$. One can then show with Eqs. (13-15) that the spinor orbitals Φ_n are orthonormal in the usual sense

$$\begin{aligned} (\Phi_n | \Phi_m) &= \int_{-\infty}^{\infty} \Phi_n^\dagger(x, t)\Phi_m(x, t)dx \\ &= \sum_{s=\pm 1} \int_{-\infty}^{\infty} \phi_n^*(x, s; t)\phi_m(x, s; t)dx \\ &= \frac{1}{2} \sum_{s=\pm 1} \int_{-\infty}^{\infty} u_n^*(x, s; t)u_m(x, s; t)dx = \delta_{nm}, \end{aligned} \quad (16)$$

in spite of their discontinuities at the X-junctions $x = L_1$ and $x = L_2$. Note that the orthonormality of the u_n holds for each fixed s (separately in each arm), whereas the orthonormality relation for the Φ_n involves both summation over s and integration over x . This is to be expected physically, since the X-junctions mix probability density between both arms. Using the Slater determinantal expression for Ψ_F in terms of the $\phi_n(x, s; t)$ and the fact that $|\Psi_B|^2 = |\Psi_F|^2$, it then follows that the single-particle density for both the Bose and Fermi systems is

$$\rho(x, s; t) = \sum_{n=0}^{N-1} |\phi_n(x, s; t)|^2. \quad (17)$$

To recapitulate, to generate the density profiles we first solve the TDSE for each $u_n(x, s, t)$, $n = 1, \dots, N$ in both arms, which does not involve the X-splitter boundary conditions. Next the orbitals $\phi_n(x, s; t)$ at the detector are constructed from the boundary condition (15), and finally the density profile is obtained from Eq. (17) above.

IV. ANALYTICAL SOLUTION

Hänsel *et al.* [16] have demonstrated a magnetic conveyor belt for atoms that could be used to launch an

atomic gas into interferometer, and recently transport of BECs by optical tweezers has been achieved by Gustavson *et al.* [24], who suggested that this technique could be used to load a BEC into a “waveguide on a chip”. We simulate the tweezer loading method by choosing the N -fermion wave function in the entrance or upper arm $s = +1$ in Fig. 1 as the ground-state of a harmonic trap of frequency ω with an overall translational velocity $v_x = \hbar k/m$, k being the longitudinal wavevector. The time when the Fermi wavepacket is released from the optical trap into the entrance arm is taken as the time origin $t = 0$ and the position of the packet-center at that instant is taken as the space origin $x = 0$. Then, the orthonormal orbitals defining the initial condition in (12) are conveniently chosen to coincide with the lowest N Hermite-Gaussians

$$u_n(x) = C_n e^{-x^2/2x_{osc}^2} H_n\left(\frac{x}{x_{osc}}\right) e^{ikx}$$

$$C_n = \frac{1}{\pi^{1/4} \sqrt{2^n n! x_{osc}}}, \quad (18)$$

where the N -fermion ground-state has one particle in each of the first N modes, and $x_{osc} = \sqrt{\hbar/m\omega}$ as before. The Fermi-wavevector associated with this N -atom ground-state is $k_F = \sqrt{2N}/x_{osc}$ [25, 26], and this serves as a measure of the wavevector on the highest occupied plane-wave orbital. We assume throughout that $k \gg k_F$ so that the center-of-mass velocity v_x of the atomic wavepacket exceeds the expansion of the wavepacket after it is released.

Our goal in this paper is to examine the response of the double-X interferometer to a variety of perturbations V_s . An interesting choice of perturbing potentials in the interferometer arms is one which is a delta-function pulse in time, $V_s(x, t) = \hbar\Lambda_s(x)\delta(t-t_0)$. Then, the orbitals just after such a perturbation are related to those just before by a spatially varying phase-shift $\Lambda_s(x)$:

$$u_n(x, s; t_0^+) = e^{-i\Lambda_s(x)} u_n(x, s; t_0^-), \quad L_1 < x < L_2. \quad (19)$$

Such an approach was used by Rojo, Cohen, and Berman to study the response of a Tonks gas to a delta-pulsed optical lattice potential [25], and we have used it more recently to investigate gray solitons in a Tonks gas [12]. It is an idealization to zero pulse length of phase imprinting techniques used in a number of recent experiments [27, 28, 29].

As a simple but concrete example, suppose that an external force acting on the interferometer exerts a different impulsive force $F_s = s\hbar[k_p + 2Qx]\delta(t-t_0)$ on each arm at a time t_0 at which the wavepackets are located within the interferometer. (We split the impulsive force between the two arms for ease in the analytic solution but the same physics arises if the force is applied to one arm). The force term proportional to k_p represents a spatially uniform force, whereas the term proportional to Q represents a spatially inhomogeneous force. The corresponding potential is $V_s(x, t) = \hbar\Lambda_s(x)\delta(t-t_0)$ with

$$\Lambda_s(x, t) = -s[\varphi/2 + k_p x + Qx^2]\delta(t-t_0), \quad (20)$$

where φ is a phase difference between the two interferometer arms due, for example, to the Sagnac effect if the interferometer is rotating. The factor $s = \pm 1$ means that the impulse is oppositely directed in the left and right arms. In the absence of a quadratic phase variation, $Q = 0$, via the equivalence principle this can be viewed as a simple model of a detector of rotational acceleration, an “atom gyroscope”.

The details of the time evolution of each orbital $u_n(x, s; t)$ in either arm from the time of loading until the time of detection are given in the Appendix: The expressions for these orbitals are somewhat cumbersome, but in general they can be written in the form $u_n(x, s; t) = U_n(x, t) \exp(i\xi_n(x, s, t))$, where U_n are real Hermite-Gaussian functions and ξ_n are phase factors, so $|u_n|^2 = |U_n|^2$. The time-evolution is the same in each arm until the time $t = t_0$ when the pulses are applied. That time is chosen so that the pulses are well contained in the interferometer arms and the amplitude of the wavepacket at the junctions is negligible (see Fig. 2). Thus for subsequent propagation the extra phase (19) acquired by each orbital due to the pulsed potentials can be taken to extend over all values of x although the potentials are limited to the lengths of the interferometer arms only.

If the potentials have no quadratic spatial dependence $Q = 0$, the phase acquired is the same for each orbital, as seen from Eq. (A5) in the Appendix. In that case the densities in the upper arm ($s = +1$) and the lower arm ($s = -1$) can be expressed in terms of real-valued orbitals U_n centered at $x_{\pm} = x_0 + \hbar(k \pm k_p)(t - t_0)/m$, see Eq. (A6):

$$\rho(x, \pm 1; t) = \frac{1}{4} \sum_{n=0}^{N-1} [U_n^2(x - x_+, t) + U_n^2(x - x_-, t)]$$

$$\mp \frac{1}{2} \cos[\theta(x, t)] \sum_{n=0}^{N-1} U_n(x - x_+, t) U_n(x - x_-, t), \quad (21)$$

where $x_0 = v_x t_0$ is the position of the center of the packets at the scaled time of application of the pulse $\tau_0 = \omega t_0$, and x_{\pm} the centers of the wavepackets in each arm at the time of detection $\tau = \omega t$. The spatial phase-modulation θ due to interference and the period λ of that modulation are given by

$$\theta(x, t) = \varphi + 2k_p \left[(x - x_m) \frac{1 + \tau_0 \tau}{1 + \tau^2} + x_0 \right]$$

$$\lambda = \left(\frac{\pi}{k_p} \right) \frac{1 + \tau^2}{1 + \tau_0 \tau}, \quad (22)$$

where $x_m = (x_+ + x_-)/2$ is the mean position of the recombined wavepackets at the time of detection. The exact analytic solution (21) will be used in the following sections to evaluate the response of the double-X interferometer to the input atom wavepacket under varying applied perturbations.

Equation (21) for the density profile in each arm has an illustrative limiting case. For small applied wavevectors

$k_p \ll k$, the centers of the wavepackets do not separate much $x_{\pm} \approx v_x t$, and we have $U_n(x - x_+, t) \simeq U_n(x - x_-, t)$. In this limit the density in each arm becomes

$$\rho(x, \pm 1; t) \simeq \frac{1}{2} [1 \mp \cos[\theta(x, t)]] \sum_{n=0}^{N-1} U_n^2(x - x_+, t), \quad (23)$$

this expression being exact for $k_p = 0$. The factor $\sum U_n^2(x - x_+, t)$ is the density profile of the expanding Tonks gas, and is identical in the present approximation to that in the absence of the applied perturbation. Thus, for $k_p \ll k$ the response of the interferometer to the perturbation is in the spatially dependent phase factor $\theta(x, t)$. For the case $k_p = 0$ we have $\theta(x, t) = \varphi$, so the densities in each arm do not show spatial fringes, and we may integrate the density over x to find *exact* expressions for the number of atoms N_{\pm} in each output arm

$$N_{\pm} = \frac{N}{2} [1 \mp \cos(\varphi)]. \quad (24)$$

Then if we set $\varphi = \varphi_b + \Delta\varphi$, where φ_b is a bias phase-shift, created, for example, using an optical dipole potential applied to one arm, and $\Delta\varphi$ is a phase difference between the two arms due to the Sagnac effect, we find $(N_+ - N_-) = -N \cos(\varphi_b + \Delta\varphi)$. Setting $\varphi_b = \pi/2$ we obtain

$$(N_+ - N_-) = N \sin(\Delta\varphi). \quad (25)$$

Thus, measuring the difference in numbers of atoms exiting the two interferometer arms provides a measure of the excess phase-shift $\Delta\varphi = 2m\omega_R A/\hbar$ due to rotation, for example, where ω_R is the rotation frequency and A the enclosed area of the interferometer.

When $k_p \neq 0$ Eq. (21) shows that the output density in each arm can exhibit spatial fringes with period λ as the phase $\theta(x, t)$ becomes x -dependent. The fringes become apparent when $2x_F/\lambda = 2\sqrt{2N}x_{osc}/\lambda > 1$, so that there is more than one fringe under the atomic wavepacket width. The condition on the perturbing wavevector to observe fringes is therefore

$$\frac{k_p}{k} > \frac{1}{2\sqrt{2N}} \frac{\pi}{(kx_{osc})} \left(\frac{1 + \tau^2}{1 + \tau_0\tau} \right). \quad (26)$$

However, for momentum kicks k_p such that the distance $(x_+ - x_-) = 2\hbar k_p(t - t_0)/m$ between the wavepacket centers in the two arms becomes greater than the width $x_F\sqrt{1 + \tau^2}$ of the expanding Tonks gas at scaled detection time $\tau = \omega t$, then the fringes will tend to vanish as the exiting wavepackets from the two arms no longer overlap. This yields the following condition for the exiting wavepackets to not overlap

$$\frac{k_p}{k} > \sqrt{\frac{N}{2}} \frac{x_{osc}\sqrt{1 + \tau^2}}{(x_m - x_0)}, \quad (27)$$

where x_m is the mean position of the recombined wavepackets at the scaled time $\tau = \omega t$ of detection. Furthermore, if $\tau \approx \omega(x_m/v_x) \ll 1$, then the atomic wavepacket will not spread much during its passage through the interferometer.

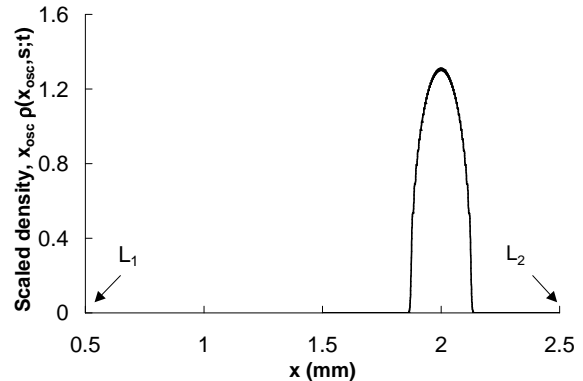


FIG. 2: The shape of the wavepacket in *either* arm before the pulses are applied, shown when the packet center is at $x_0 = 2$ mm .

V. NUMERICAL RESULTS

In this section we present numerical solutions from our model to illustrate the interferometric response of the double-X atom interferometer to a variety of imposed perturbations. These illustrations are intended to display some interesting features of the theory and not to serve as detailed study of a particular mode of interferometer operation, eg. a rotation sensor.

For our numerical study of the interferometric response of the double-X interferometer we choose parameters corresponding to the optical-tweezer loading experiment of Ref. [24], with longitudinal trap frequency $\nu = 4\text{Hz} \Rightarrow \omega = 25.1\text{ Hz}$, which gives an oscillator length of $x_{osc} = 1.04 \times 10^{-2}\text{ mm}$ for sodium atoms. The optimal transfer velocity of 70 mm/s is chosen to be the initial velocity v_x of the wavepacket launched into the interferometer, which corresponds to a wavevector $k = 267x_{osc}^{-1}$. The arm-lengths in the interferometer are fixed by taking $L_1 = 0.5\text{ mm}$, $L_2 = 2.5\text{ mm}$ and the region of detection to be centered at $x_d = 3\text{ mm}$, 0.5 mm beyond the X-recombiner, see Fig. 1. Figure 2 shows the density in each of the two interferometer arms for $N = 51$ atoms just before the perturbing pulse is applied, and the wavepacket is seen to be well contained between the two X-splitters at L_1 and L_2 . In the following discussion the output atom densities are calculated around the point of detection $x_m = 3\text{ mm}$.

The response of the atom interferometer to a net imposed phase-shift φ between the two arms has already been addressed in the discussion leading to Eq. (25), so here we set $\varphi = 0$ and look at the effects of an applied force. Figure 3 shows the output density profiles in the upper ($s = +1$) and the lower ($s = -1$) arms of the interferometer for an initial wavepacket of $N = 51$ atoms moving with velocity $v_x = 70\text{ mm/s}$, pulsed force ap-

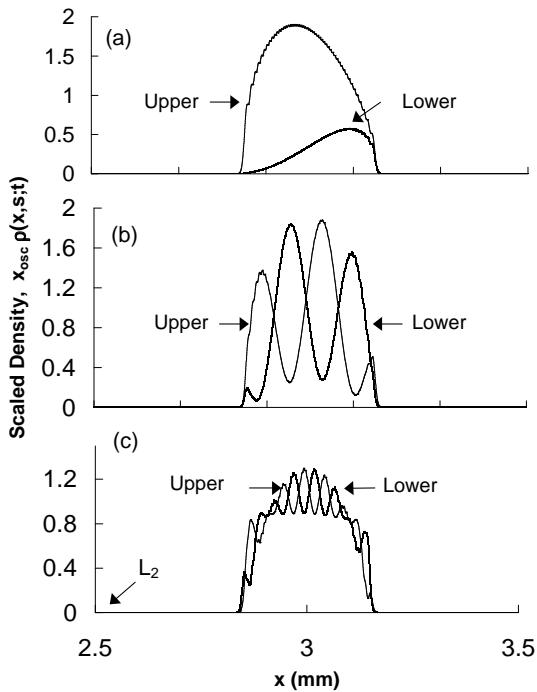


FIG. 3: Density profile of the recombined wavepackets in the upper ($s = +1$) and the lower ($s = -1$) arms for an initial wavepacket of 51 atoms moving with velocity $v_x = 70$ mm/s, and the pulsed potentials $V_s(x, t)$ applied when $x_0 = 2$ mm: (a) $k_p/k = 10^{-4}$ and $Q = 0$, (b) $k_p/k = 10^{-3}$ and $Q = 0$ and (c) $k_p/k = 10^{-3}$ and $Q/k = 5 \times 10^{-4} \text{ mm}^{-1}$.

plied at $x_0 = 2$ mm with (a) $k_p/k = 10^{-4}$ and $Q = 0$, (b) $k_p/k = 10^{-3}$ and $Q = 0$ and (c) $k_p/k = 10^{-3}$ and $Q/k = 5 \times 10^{-4} \text{ mm}^{-1}$. For a spatially uniform force ($Q = 0$) the condition (26) to observe fringes yields $k_p/k > 0.6 \times 10^{-3}$, and this is consistent with case (a) which shows no fringes $k_p = 10^{-4}$, and case (b) for $k_p = 10^{-3}$ which shows a couple of fringes. Thus, the period of the density fringes in each arm can act as a measure of the wavevector of the applied force via Eq. (22). However, as shown in Fig. 3(c), which is the same as (b) except with $Q \neq 0$, if the force has a spatially non-uniform component the visibility fringe can be reduced. We have found that the density fringes are sensitive to small spatially inhomogeneous components of the applied force. As the wavevector k_p of the applied perturbation is further increased beyond that used in Fig. 3(b), again with $Q = 0$, the number of density fringes increases but eventually their contrast decreases. In particular, according to the condition (27) if $k_p/k > 0.05$ then the exiting atom wavepackets no longer overlap and interference fringes are not possible.

As a second example, Fig. 4 shows the response of

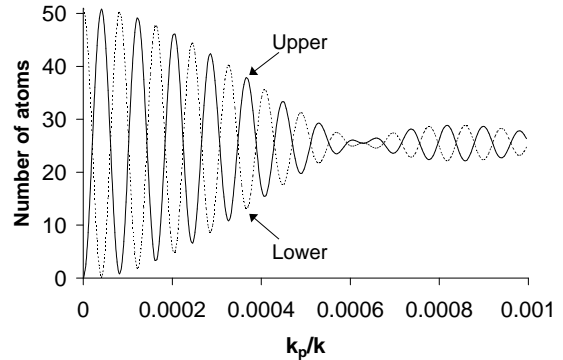


FIG. 4: Number of atoms in the upper ($s = +1$) and the lower arms as a function of linear pulse strength k_p , with $Q = 0$ and with the time of application of the pulses $V_s(x, t)$ fixed at when the packet centers are at $x_0 = 2$ mm. The initial wavepacket has 51 atoms moving with velocity $v_x = 70$ mm/s.

the interferometer to a force of varying wavevector k_p for $x_0 = 2$ mm and $N = 51$ as before. (Keeping the position or time of application of the applied force fixed is somewhat artificial but serves to illustrate our theory). In particular, the figure shows the number of atoms exiting each arm as a function of k_p . For $k_p/k \ll 0.6 \times 10^{-3}$, so that there are no density fringes under the atom wavepacket, the atom numbers exhibit almost complete periodic oscillations. We can understand this behavior from Eq. (23) for the densities in each arm: When $k_p/k \ll 0.6 \times 10^{-3}$ the phase $\theta(x, t)$ varies little over the spatial extent of the atom wavepacket, in which case the integrated atom numbers in each arm are given to a good approximation by Eq. (24) with φ replaced by $2k_p x_0$, which shows periodic exchange. In contrast, for $k_p/k > 0.6 \times 10^{-3}$ the atom number oscillations are much smaller in amplitude and centered around 50:50 splitting. In the regime $k_p/k \gg 0.6 \times 10^{-3}$ the phase $\theta(x, t)$ varies significantly over the spatial extent of the atom wavepacket, and upon integrating Eq. (23) over x to obtain the atom numbers in each arm, the cosine terms will tend to integrate to zero due to their oscillatory nature, giving 50:50 splitting.

VI. SUMMARY AND CONCLUSIONS

In summary, by introducing a generalization of the Fermi-Bose mapping for coupled waveguides we have developed the theory of a double-X atom interferometer in the Tonks-gas limit [8, 9] of tight transverse confinement and impenetrable interactions between the atoms. We believe this is a significant development in view of cur-

rent efforts to create 1D integrated atom interferometers, and in waveguide on a chip technology in general, for inertial and other sensors. In particular, we have calculated the interferometric response of the double-X device for a variety of imposed external perturbations to illustrate the utility of our theory. A key result of our work is to show that despite the fact that we are in the Tonks-gas limit, where the condensed fraction of the initial gas tends to zero for large number of atoms, the interferometer can still show high visibility density fringes at the output. That is, our results show the 1D waveguide devices with ultracold but non-condensate atom sources can still exhibit a high degree of first-order coherence. Furthermore, due to the Fermi-Bose mapping our results apply equally well to a spin-polarized fermionic atom source, for which s-wave scattering is absent.

Acknowledgments

We are grateful to Mara Prentiss and Brian Anderson for helpful discussions. This work was supported by Office of Naval Research grant N00014-99-1-0806 and the US Army Research Office.

APPENDIX A: TIME EVOLUTION OF THE ORBITALS

In the absence of external potentials the time evolved orbitals $u_n(x, s; t')$ at time $t = t' + \Delta t$ are obtained from those at time t by applying the retarded free particle Green's function

$$u_n(x, s; t) = \frac{1}{\sqrt{2\pi i\omega\Delta t}} \int_{-\infty}^{\infty} dx' u_n(x', s; t') e^{-\frac{(x-x')^2}{2i\omega\Delta t}} \quad (\text{A1})$$

For brevity in notation we introduce the scaled variables $\tau_0 = \omega t_0$ for the time of application of the pulse, $\tau = \omega t$ for the time of detection, and $\tau_d = \omega(t - t_0)$. We also introduce Greek letters to designate the scaled variables $\chi = x/x_{osc}$ and $\kappa = kx_{osc}$ and $\Omega = Qx_{osc}^2$. The free propagation of each orbital $u_n(x, s; t)$ via either arm is identical up until the instant $t = t_0^-$ before the pulses are applied

$$u_n(x, s; t_0^-) = \frac{C_n e^{-i\frac{\kappa^2\tau_0}{2}}}{\sqrt{1+i\tau_0}} \left[\frac{1-i\tau_0}{1+i\tau_0} \right]^{n/2} \times e^{i\kappa\chi} e^{-\frac{(\chi-\chi_0)^2}{2(1+i\tau_0)}} H_n \left(\frac{\chi-\chi_0}{\sqrt{1+\tau_0^2}} \right), \quad (\text{A2})$$

where the new center of the wavepacket is at $\chi_0 = \kappa\tau_0$. After the pulsed potentials $V_s(x, t)$ are applied the orbitals acquire an additional space-dependent phase different in each arm

$$u_n(x, s; t_0^+) = e^{is(\kappa_p\chi + \Omega\chi^2)} u_n(x, s; t_0^-). \quad (\text{A3})$$

Evaluating the subsequent free propagation till a time $t > t_0$ after the wavepacket from each arm has completely passed through the recombiner, one finds the functional form of the modes coming from the two arms to be

$$u_n(x, \pm 1; t) = \frac{C_n e^{-\frac{i}{2}\kappa^2\tau_0}}{\sqrt{(1 \pm 2\Omega\tau_d) + i(\tau \pm 2\tau_0\Omega\tau_d)}} \times \left[\frac{(1 \pm 2\Omega\tau_d) - i(\tau \pm 2\tau_0\Omega\tau_d)}{(1 \pm 2\Omega\tau_d) + i(\tau \pm 2\tau_0\Omega\tau_d)} \right]^{n/2} e^{\frac{F_{\pm}(\chi, \tau, \tau_0)}{G_{\pm}(\chi, \tau, \tau_0)}} \times H_n \left(\frac{\chi - [\chi_0 + (\kappa_{\pm} \pm 2\chi_0\Omega)\tau_d]}{\sqrt{[1 \pm 2\Omega\tau_d]^2 + [\tau \pm 2\tau_0\Omega\tau_d]^2}} \right), \quad (\text{A4})$$

with $\kappa_{\pm} = \kappa \pm \kappa_p$, and the argument of the exponential is given by

$$F_{\pm}(\chi, \tau, \tau_0) = -(1 \pm 2\Omega\tau_d)\chi_0^2 - \kappa_{\pm}\tau_d[2\chi_0 + i\kappa_{\pm}(1 + i\tau_0)] + 2\chi[\chi_0 + i\kappa_{\pm}(1 + i\tau_0)] - [(1 \pm 2\Omega\tau_0) - i(\pm 2\Omega)]\chi^2$$

$$G_{\pm}(\chi, \tau, \tau_0) = 2[(1 + i\tau) + (\pm 2\Omega)\tau_d(1 + i\tau_0)].$$

When the potential has only a linear dependence on x i.e. $\Omega = 0$ this expression acquires a more transparent form

$$u_n(x, \pm 1; t) = \frac{C_n e^{-\frac{i}{2}(\kappa_{\pm}^2\tau_d + \kappa^2\tau_0)}}{\sqrt{1+i\tau}} \left[\frac{1-i\tau}{1+i\tau} \right]^{n/2} \times e^{i\chi\kappa_{\pm}} e^{-\frac{[\chi - (\kappa_{\pm}\tau_d + \chi_0)]^2}{2(1+i\tau)}} H_n \left(\frac{\chi - (\chi_0 + \kappa_{\pm}\tau_d)}{\sqrt{1+\tau^2}} \right). \quad (\text{A5})$$

This expression contains a phase-independent factor which is a Hermite-Gaussian centered at $x_{\pm} = x_0 + \kappa_{\pm}\tau_d$ with width $\sqrt{1+\tau^2}$, that we represent in terms of unscaled variables

$$U_n(x - x_{\pm}, t) = \frac{C_n e^{-\frac{[x-x_{\pm}]^2}{2[1+(\omega t)^2]}}}{[1+(\omega t)^2]^{1/4}} H_n \left(\frac{x - x_{\pm}}{x_{osc}\sqrt{1+(\omega t)^2}} \right). \quad (\text{A6})$$

- [1] M. Key *et al.*, Phys. Rev. Lett. **84**, 1371 (2000).
- [2] D. Muller *et al.*, Phys. Rev. Lett. **83**, 5194 (1999).
- [3] N.H. Dekker *et al.*, Phys. Rev. Lett. **84**, 1124 (2000).
- [4] J.H. Thywissen *et al.*, Phys. Rev. Lett. **83**, 3762 (1999).
- [5] E.A. Hinds *et al.*, Phys. Rev. Lett. **80**, 645 (1998).

- [6] P.R. Berman, ed., *Atom Interferometry* (Academic Press, Boston, 1997).
- [7] J. Schmiedmayer, Eur. Phys. J. D **4**, 57 (1998).
- [8] M. Olshanii, Phys. Rev. Lett. **81**, 938 (1998).
- [9] D.S. Petrov *et al.*, Phys. Rev. Lett. **85**, 3745 (2000).

- [10] M. Girardeau, *J. Math. Phys.* **1**, 516 (1960).
- [11] M.D. Girardeau, *Phys. Rev.* **139**, B500 (1965), see particularly Secs. 2, 3, and 6.
- [12] M.D. Girardeau and E.M. Wright, *Phys. Rev. Lett.* **84**, 5691 (2000).
- [13] M.D. Girardeau and E.M. Wright, *Phys. Rev. Lett.* **84**, 5239 (2000).
- [14] M.D. Girardeau, E.M. Wright, and J.M. Triscari, *Phys. Rev. A* **63**, 033601 (2001).
- [15] R. Folman *et al.*, *Phys. Rev. Lett.* **84**, 4749 (2000).
- [16] W. Hänsel, J. Reichel, P. Hommelhoff, and T. W. Hänsch, *Phys. Rev. Lett.* **86**, 608 (2001).
- [17] H. Ott *et al.*, *Phys. Rev. Lett.* **87**, 230401 (2001).
- [18] D. Cassettari *et al.*, *Phys. Rev. Lett.* **85**, 5483 (2000).
- [19] E. Andersson *et al.*, *Phys. Rev. Lett.* **88**, 100401 (2002).
- [20] M.O. Scully and J.P. Dowling, *Phys. Rev. A* **48**, 3186 (1993).
- [21] M.O. Scully and M.S. Zubairy, *Quantum Optics* (Cambridge University Press, 1997), pp. 494 ff.
- [22] R. Loudon, *Phys. Rev. A* **58**, 4904 (1998).
- [23] E. B. Kolomeisky, T. J. Newman, J. P. Straley, and Xiaoya Qi, *Phys. Rev. Lett.* **85**, 1146 (2000).
- [24] T.L. Gustavson *et al.*, *Phys. Rev. Lett.* **88**, 020401 (2002).
- [25] A.G. Rojo *et al.*, *Phys. Rev. A* **60**, 1482 (1999).
- [26] K. K. Das, *et al.*, *cond-mat/0202189* (2002).
- [27] S. Burger *et al.*, *Phys. Rev. Lett.* **83**, 5198 (1999).
- [28] J. Denschlag *et al.*, *Science* **287**, 97 (1999).
- [29] J.M. Vogels *et al.*, *Phys. Rev. Lett.* **88**, 060402 (2002).